THE ASTROPHYSICAL JOURNAL, 507:745–758, 1998 November 10

HCO^+ IN THE STARBURST GALAXY M82

E. R. SEAQUIST AND D. T. FRAYER[1]
Department of Astronomy, University of Toronto, Toronto, Ontario M5S 3H8, Canada

AND

M. B. BELL
National Research Council of Canada, 100 Sussex Drive, Ottawa, Ontario K1A 0R6, Canada
Received 1998 April 27; accepted 1998 June 18

ABSTRACT

We report observations and an analysis of the distribution of HCO^+ (1–0) and HCO^+ (4–3) emission in the central 1 kpc star-forming region of M82. Comparisons are made with other star formation indicators such as the millimeter continuum, the distribution of radio supernova remnants, and the molecules CO and OH. In a broad sense, the HCO^+ is distributed in a way similar to the CO, although there are noticeable differences in detail, including an inward displacement of spiral arm emission relative to CO. A comparison of the position-velocity plots for CO, HCO^+ (1–0), HCO^+ (4–3), and ionized gas, with orbits expected in the presence of the nuclear bar, suggest an inward transfer of gas associated with star formation toward the nucleus.

The HCO^+ (4–3)/(1–0) line ratios are comparatively uniform in the observed region, and according to a large velocity gradient analysis, reflect mean gas densities in the range 10^4–10^5 cm^{-3} for kinetic temperatures in the range 20–60 K. The comparative uniformity of these conditions and the low filling factor suggest that each sampled point comprises a large number of clouds occupying a broad range of density, and possibly temperature. We briefly examine fractal-type models in the context of the HCO^+ data as an alternative way to analyze molecular line emission in M82.

Subject headings: galaxies: individual (M82) — galaxies: ISM — galaxies: nuclei — galaxies: starburst

1. INTRODUCTION

The starburst galaxy M82 continues to be the focus of many studies intended to elucidate the star-forming mechanism. Its proximity (3.25 Mpc) and intense nuclear star formation activity in the inner 1 kpc make it an ideal candidate for this purpose. Much attention has been focused on the properties of the molecular clouds in this region, and this topic is also the focus of the present paper. According to the schematic in Figure 13 of Achtermann & Lacy (1995), for example, the molecular gas is concentrated in a ring of radius about 210 pc, and there is an inner ring of ionized gas with a radius of about 80 pc. On the basis of the position-velocity (*p-v*) maps for CO, Shen & Lo (1995) have identified two possible spiral arms, one at radius 125 pc and the other at 390 pc. Based on their CO interferometric maps, Shen & Lo found that the molecular gas comprises about 60 molecular clouds with diameters ranging from 10 to 100 pc, with velocity widths ranging upward from 7 km s^{-1}, similar to clouds in our Galactic center. Based on interferometric studies of denser gas reflected in the distribution of HCN, Brouillet & Schilke (1993) found similar cloud properties, and also noted their similarity to giant molecular cloud complexes in our Galaxy.

Here we extend the investigation of the properties of the molecular gas in M82 by reporting and discussing the distribution of HCO^+ in this region. The molecule HCO^+ has a comparatively high critical density (approximately 10^5 and 10^7 cm^{-3} for the (1–0) and (4–3) transitions, respectively). Thus this molecule is preferentially excited by denser molecular gas, comparable to that responsible for the excitation of HCN. In addition, however, the HCO^+ intensities may be affected by cosmic-ray ionization, and its excitation may depend on a number of factors that would not affect HCN (e.g., Richardson et al. 1988). We have mapped this molecular ion in the (1–0) and (4–3) transitions, representing the initial phase of a larger study of tracers of dense gas in M82. This study complements other molecular line studies as well as our earlier investigation of the H41α recombination line, which revealed structures associated with dense ionized gas (Seaquist et al. 1996). Some of these structures appear to participate in the outflow from the starburst region. These observations also revealed velocity displacements between the ionized and HCO^+-emitting gas, a further indication either of outflow or of motions by the two species on different orbits. Although previous papers have reported measurements of both HCO^+ transitions (e.g., Stark & Wolff 1979; Carlstrom 1988; Rieu, Nakai, & Jackson 1989; Wild et al. 1992), the results reported here are the first to provide a comparison of HCO^+ at the (1–0) and (4–3) transitions based on fully sampled maps.

As part of this study, we also examine the relationship between the millimeter radio continuum and the molecular gas inferred from both HCO^+ and CO in order to investigate the Schmidt law relating star formation rate to gas density. A particular benefit of using the millimeter continuum, which measures the star formation rate through its association with thermal emission from ionized gas, is its freedom from obscuration by dust in M82.

2. OBSERVATIONS

Observations of the HCO^+ (1–0) line were made with the five-element millimeter array of the Owens Valley Radio Observatory (OVRO) during four observing periods

[1] Current address: Department of Astronomy, 105-24 Caltech, Pasadena, CA 91125.

throughout 1993–1994, and observations of the HCO^+ (4–3) line were made with the James Clerk Maxwell Telescope (JCMT) during 1995 December.

2.1. *The* HCO^+ (1–0) *Observations*

These data were acquired at OVRO simultaneously with data on the H41α line, which were reported by Seaquist et al. (1996). The reader is referred to this paper for details on the observational procedures. The HCO^+ (1–0) line at 89.1885 GHz was observed in the lower sideband, and the H41α line at 92.0344 GHz in the upper sideband. The dates and lower sideband system parameters for these observations are shown in Table 1. Three different array configurations were used over the four observing periods, providing a resultant angular resolution of approximately 3.″5. The spectrometer combined four bands of 32 independent spectral line channels each, after on-line Hanning smoothing. After deletion of two channels at the edge of each band, the final number of channels was 112 spread over a bandwidth of 448 MHz, providing a channel separation of 4 MHz. In terms of velocity, the total coverage was 1408 km s^{-1} with a channel separation of 13.46 km s^{-1}. Weather conditions were generally good to excellent during the observations, with the exception of the last session on 1994 April 28. The rms pointing error was about 4″ in each coordinate except for sunrise and sunset, when the errors were larger. In all cases the pointing errors were small compared to the size of the primary beam, which is about 88″ (FWHM).

2.2. *The* HCO^+ (4–3) *Observations*

Observations were made of the HCO^+ (4–3) line at 356.7343 GHz on 1995 December 2 and 3 using receiver B3i on the JCMT. The observations were conducted with a spectrometer setup providing 1216 channels covering a bandwidth of 760 MHz and a channel separation of 625 kHz. These correspond to a total velocity coverage of 639 km s^{-1} and velocity resolution of 0.527 km s^{-1}, respectively. The beam size of the JCMT at the frequency of the HCO^+ (4–3) transition is 14″ (FWHM). Measurements were made at 30 positions in the central region of M82, using a 7″ grid centered on the (B1950) position R.A. = $09^h51^m42^s.34$, decl. = 69°55′00″ and aligned with the major axis of M82, which was assumed to be at P.A. 75°. The spectrometer band was centered at $V(\mathrm{LSR}) = 200$ km s^{-1}. The data were taken by beam-switching in azimuth using a beam throw of 120″and a switch rate of 7.813 Hz. This beam throw is sufficient to position the reference beam well off the source at all map positions. The average air mass was 1.73 for the observations, and the corresponding mean system temperature was 1197 K, averaged over the central 75% of the band. The telescope pointing was monitored every 1–2 hours using a strong continuum source as a calibrator, typically 3C 273 or the nearby source 0923+392. The rms pointing error was found to be 2.″1 in azimuth and 2.″6 in elevation, both substantially smaller than the beam size. The T_A^* scale was converted to main-beam brightness temperature T_{MB} using a main-beam efficiency of 0.59.

TABLE 1

PARAMETERS FOR THE OVRO OBSERVATIONS

Date	Baselines (m)	$\langle T_{\mathrm{sys}} \rangle$ (K)	Integration (minutes)
1993 Nov 15.....	20 to −67	484	525
1993 Dec 23	40 to 206	449	380
1994 Jan 29.....	15 to 119	508	645
1994 Apr 28	20 to 67	833	425

NOTE.—$\langle T_{\mathrm{sys}} \rangle$ means system temperature averaged over time and sideband.

3. RESULTS AND ANALYSIS

3.1. *The* HCO^+ (1–0) *Data*

In this section we present an overview of the results, and defer a detailed discussion of their interpretation and broader implications to § 4.

The OVRO line data are presented in Figures 1, 2, and 3. Figure 1 is a series of channel maps, Figure 2 is a position-velocity (*p-v*) plot (shown together with a similar map for CO), with position measured along the major axis, assumed to be at P.A. 75°, and Figure 3 shows the integrated brightness map, i.e., with the line emission summed over all velocity channels. For comparison, Figure 3 also shows a CO-integrated brightness map adapted from Shen & Lo (1995) and a 3 mm continuum map, published by Seaquist et al. (1996). The CO map was convolved to the resolution of the HCO^+ and 3 mm continuum OVRO maps. Figure 4 is a map of the ratio (HCO^+/CO) of the integrated brightness maps in Figure 3. This map shows the distribution of regions of enhancements (and deficiencies) of HCO^+ relative to CO emission, and is relevant for comparisons involving sites of dense molecular gas or enhancements in the abundance of HCO^+. No correction for primary-beam attenuation has been applied to the HCO^+ or continuum maps. The attenuation is estimated to be about 10% at the easternmost and westernmost extremities of the M82 emitting region ($\pm 15''$ from the phase center).

The channel maps in Figure 1 have an rms of 12 mJy, which is close to the theoretical value for thermal noise estimated from the known system temperatures and the total integration time. Figures 1 and 2 both show clearly the effect of rotation of the galaxy, and indicate a systemic velocity of 225 ± 10 km s^{-1}, in good agreement with other determinations (e.g., Weliachew, Fomalont, & Griesen 1984). The distribution of emission is broadly similar to that seen in CO (Shen & Lo 1995) and HCN (Brouillet & Schilke 1993), clearly indicating the presence of spiral features. The peak brightness on these maps is about 200 mJy per beam area, which for the 3.″25 × 3.″50 Gaussian beam corresponds to a brightness temperature of 2.9 K. Thus, if the individual clouds contributing this brightness are assumed to be optically thick with an excitation temperature of 50 K (the dust temperature), the dilution factor for the peak emission would be about 0.06. These maps therefore suggest that the HCO^+ is in the form of compact clouds heavily diluted by the telescope synthesized beam.

3.1.1. *Comparison of the Brightness Scale with Single-Dish Data*

In order to provide an assessment of missing flux in the interferometer maps due to missing short spacings, we made a comparison between our data and HCO^+ (1–0) measurements made with the Nobeyama 45 m telescope by Rieu et al. (1989). The latter observations were made with an angular resolution of 23″ at five points along the major axis of M82. The central point is at the nucleus, and the other points are offset at ±10″ and ±25″ along the major axis from the nucleus. For comparison, we convolved the OVRO maps to an angular resolution of 23″ and, from the

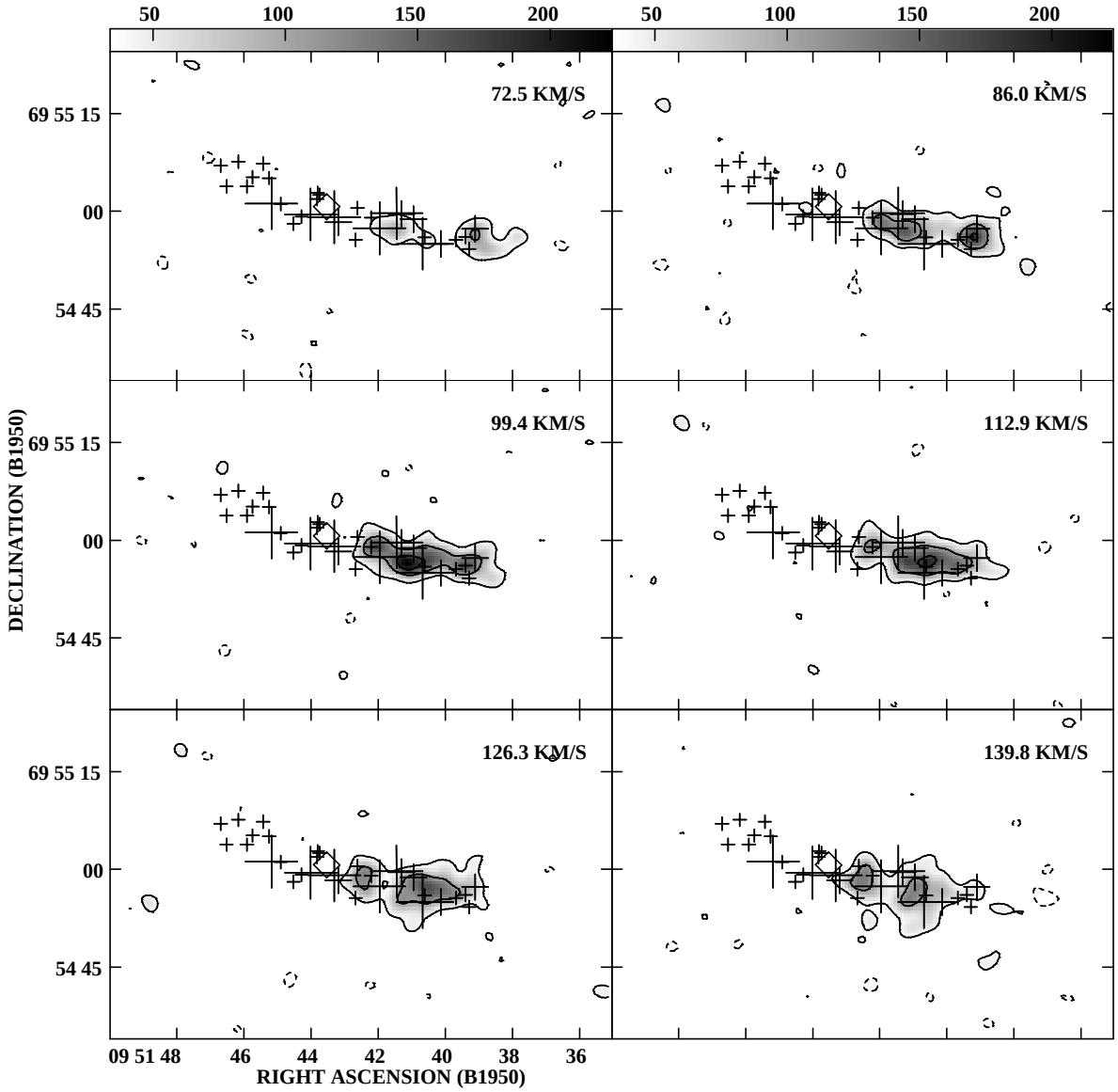

FIG. 1.—Channel maps of HCO^+ (1–0) emission in M82. Crosses refer to the locations of the radio SNRs (Kronberg et al. 1985), with size roughly proportional to the flux, and the diamond marks the position of the IR nucleus according to Dietz et al. (1986). The contour levels in flux density beam^{-1} (main-beam temperature) are 35 mJy (0.473 K) × (−1, 1, 3, 5, 7). The last image is the continuum at 92 GHz, and shows the beam size for all maps at the lower left corner. The contours for the continuum map are 3.0 mJy × (−1, 1, 2, 3, 4, 6, 8, 10, 12, 16, 20).

resulting spectral line cube, generated spectra at the positions corresponding to those of Rieu et al. (1989). The comparison between the two sets of line profiles is shown in Figure 5. Both sets of spectra are shown in units of main-beam brightness temperature (T_{MB}). A main-beam efficiency of 0.60 was used to convert the values of T_A^* plotted by Rieu et al. to the T_{MB} scale.

Figure 5 generally shows quite good agreement in the nuclear region and southwest side of M82. On the northeast side the line brightness measured by the interferometer is weaker than that measured by the 45 m telescope, particularly at the position 25 NE. The line profiles were integrated over the velocity range 0–400 km s^{-1}, and the resulting OVRO/Nobeyama line ratios for the five positions (west to east) are 0.75 ± 0.05, 0.93 ± 0.02, 0.75 ± 0.01, 0.68 ± 0.01, and 0.59 ± 0.06, where the errors refer only to the noise and do not include calibration errors. Figure 5 and the lower ratio on the east side suggest that there is an extended component on this side with velocities between 180 and 280 km s^{-1} not sampled by the interferometer. This result is confirmed by comparison with similar (unpublished) measurements made by us with the 12 m telescope of the National Radio Astronomy Observatory (NRAO) with a much larger FWHM beam size of 70″. Once again, the agreement is relatively good on the west side, but there is even more missing flux on the east side. These results place a limit on the precision achievable in the comparison between the HCO^+ (4–3) and HCO^+ (1–0) measurements, which are discussed in more detail later. However, the agreement between the interferometer and single-dish brightness measurements improve as the resolution increases, which would be expected if the reason is inadequate sampling of an extended feature. We conservatively estimate that (4–3)/(1–0) line ratios using JCMT and OVRO data smoothed to 14″ resolution would be overestimated by an average of about 25%.

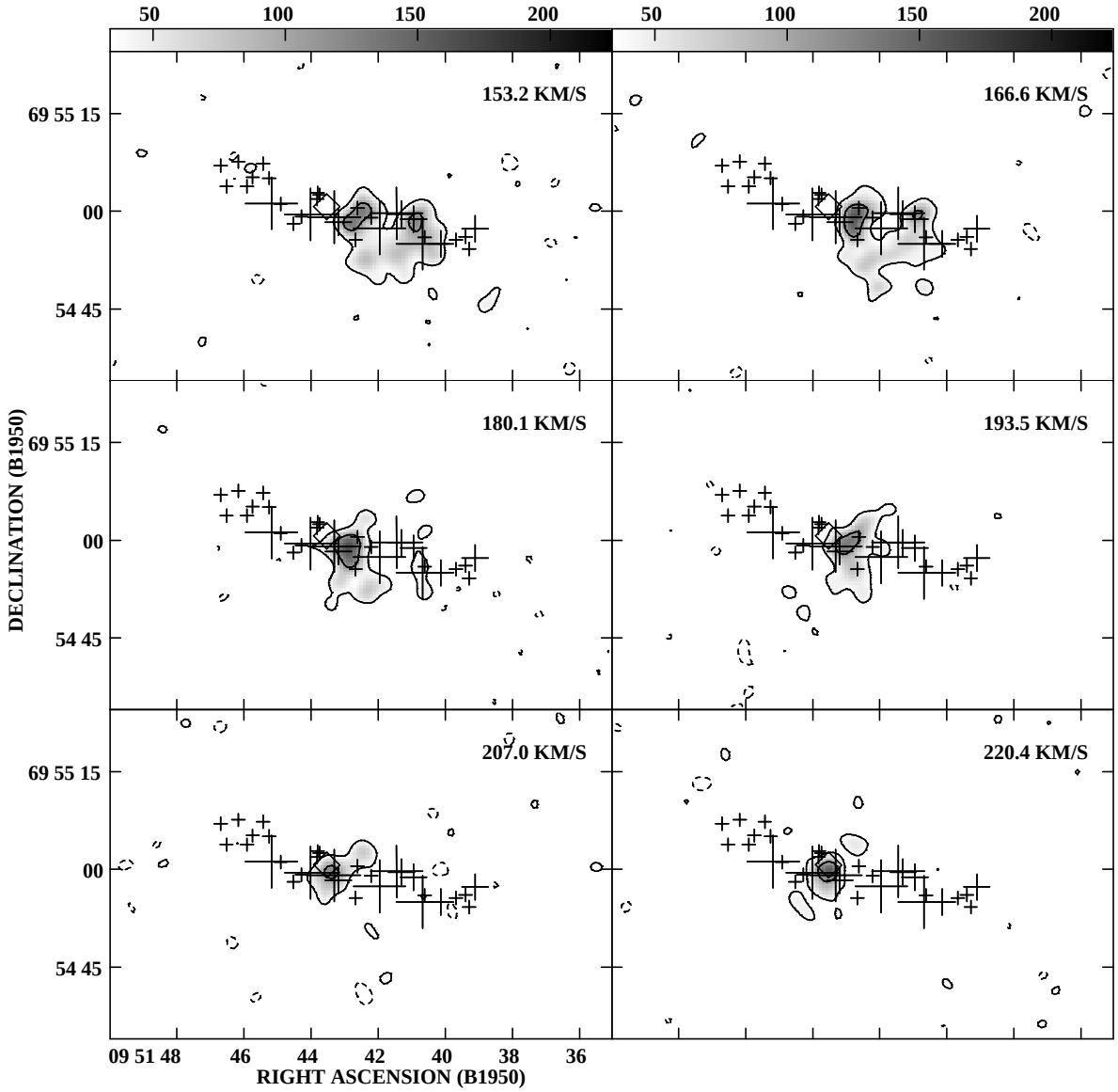

FIG. 1.—*Continued*

3.1.2. *Comparison with* CO

Overall, there appears to be a disk or torus of emission whose thickness is roughly comparable to the beam (50 pc). However, there is considerable structure in the disk, with many features corresponding to those seen in CO (Shen & Lo 1995) and HCN (Brouillet & Schilke 1993), and also there is a broad correspondence between line and continuum emission, as may be seen by comparing the maps in Figure 3. In particular, there is good qualitative correspondence between features in the HCO^+ map and features W2, W3, C1, and E2 (designations by Shen & Lo) in the CO map, and interpreted by Shen & Lo as the projections of rings or spiral arms seen tangentially. There are, however, some variations in the locations of the peak brightness, which may reflect real variations due to differences in gas distribution and/or kinematics. For example, there is a significant displacement between the peaks for the westernmost bright feature W3 as seen in HCO^+ and CO, with the former being displaced closer to the nucleus compared to the latter, placing it in closer correspondence with the continuum peak of this arm. This effect shows up most clearly in the comparisons made in Figure 3 among the different constituents. Such an effect is consistent with that expected if the star formation were occurring in preferentially denser gas at the inner edge of the arm. The same effect is not evident on the east side, where there is good agreement between the positions of corresponding features. Thus, although there is a general correspondence between features that measure the distribution of gas, there is some variation with tracer according to critical density and sensitivity to star-forming activity.

Such displacements are confirmed by a comparison between the HCO^+ and CO *p-v* plots shown in Figure 2. Note that the aforementioned peaks have distinct kinematic signatures. There is a strong correspondence between these two maps of the distribution of velocity along the major axis of M82. Shen & Lo (1995) attribute the existence of the peaks W3 (west of nucleus) and C1 (near the center) in the integrated brightness maps to "velocity crowding." However, the term may be somewhat misleading, since

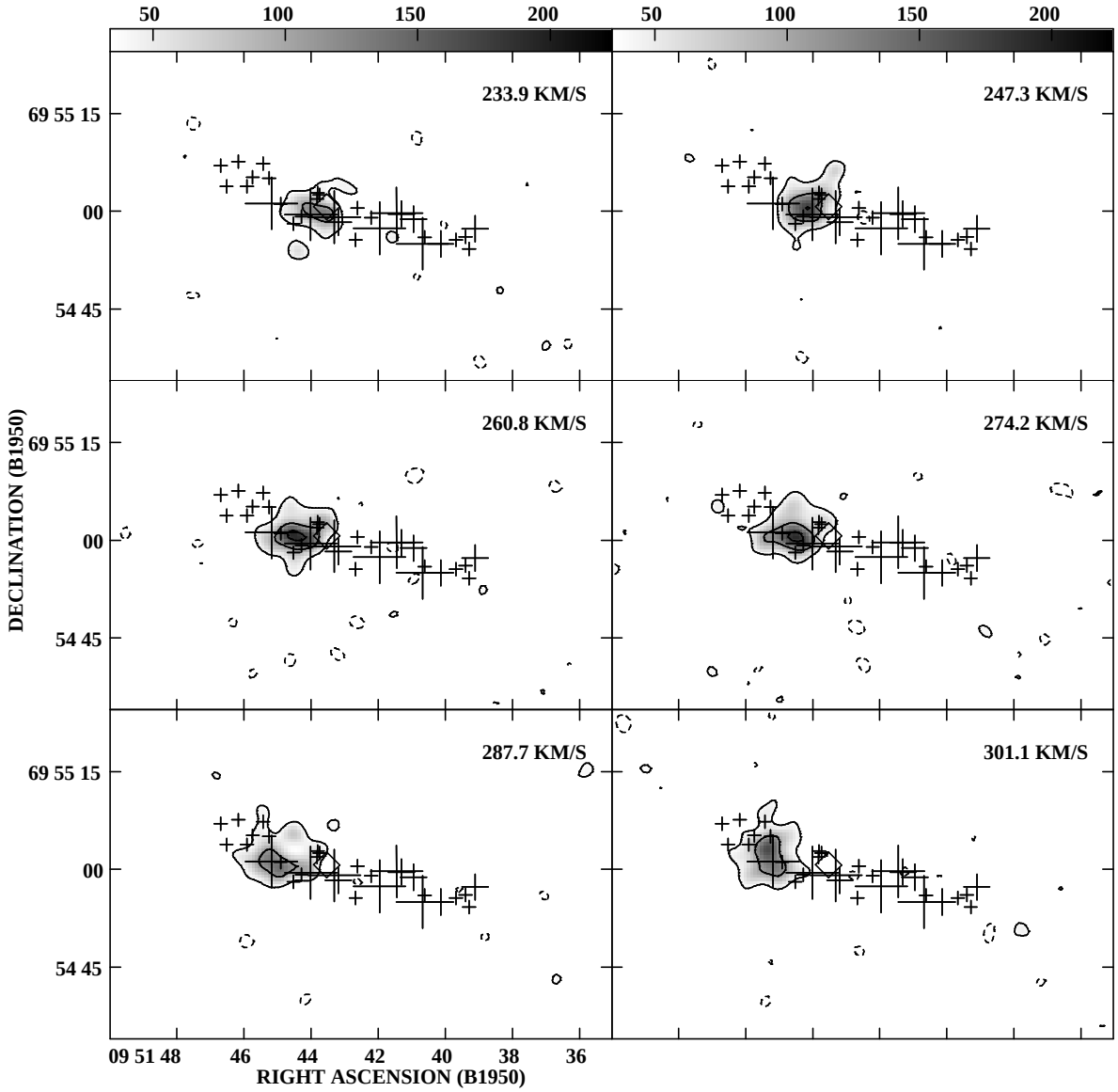

FIG. 1.—*Continued*

these peaks are visible in the *p-v* plots as structures spread out in velocity. Thus they are in fact produced by large column densities of gas. The feature C1 is associated with gas with a velocity gradient that is very steep compared with that of the general rotation curve. This steeply inclined feature is visible both in HCO^+ and CO, and may be an inner ring or spiral arm. This feature is also closely associated with a ring of ionized gas in the nuclear region, as may be seen from the diagonal solid line in Figure 2 representing the model for the ionized ring produced by Achtermann & Lacy (1995) based on observations of [Ne II] at 12.8 μm. The location of this ionized ring is also in good agreement with the location of ionized gas exhibited by [N II] λ6583, reported by Götz et al. (1990), and with observations of the H41α line by Seaquist et al. (1996). The ionized ring appears displaced toward lower velocity (or toward the east in position) relative to its counterpart in the molecular gas (see also § 4.1).

3.1.3. *Comparison with Supernova Remnants*

Figure 1 shows that there is a general correspondence between HCO^+ emission and the distribution of compact radio supernova remnants (SNRs). The latter are indicated by crosses, based on positions given by Kronberg, Biermann, & Schwab (1985). There is an apparent avoidance by SNRs of the central brightest parts of the strongest emission regions, suggesting that star formation occurs at the periphery of these complexes (see, for example, the channel maps for $V = 86$ and 328 km s^{-1}). This effect has also been pointed out by Shen & Lo (1995) in the case of CO. Although similar comparisons have been made with star clusters (e.g., Brouillet & Schilke 1993), extinction within M82 in the optical and infrared makes the interpretation less clear in this case.

Our data make it possible to test for a correlation between the sites of SNRs and the existence of dense or ionized molecular gas indicated by a preferential enhancement of the HCO^+/CO ratio shown in Figure 4. Caution must be exercised in making such a comparison because the HCO^+ and CO maps are based on a different sampling of the *u-v* plane, but this map should give a qualitative indication of the sites of highest gas density. An analysis was performed to determine whether this ratio is systematically higher at the locations of the SNRs than elsewhere. The

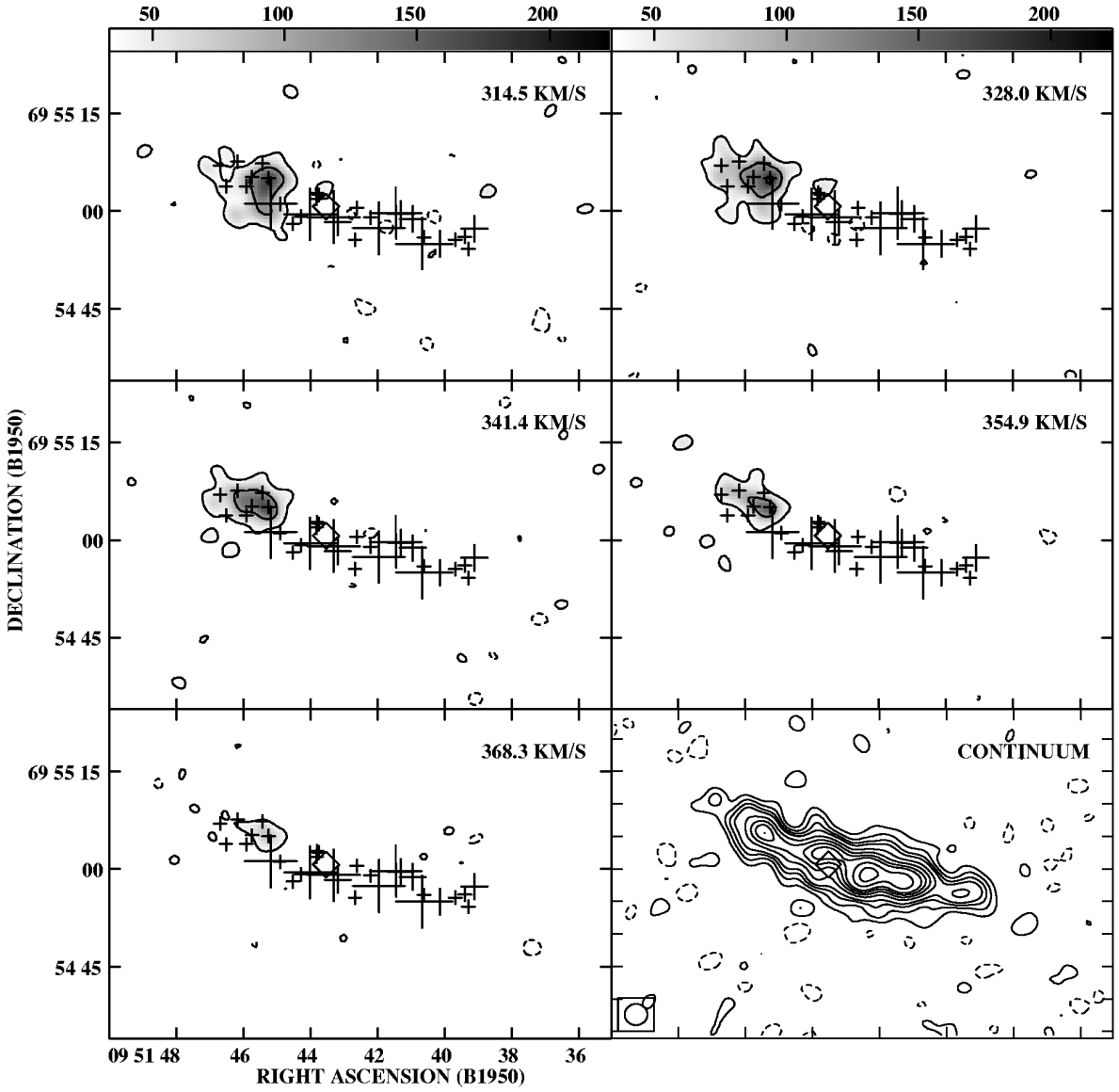

FIG. 1.—*Continued*

analysis showed that, on the whole, the distribution of the ratios sampled at the sites of SNRs is not significantly different than for points selected where there are no SNRs. Thus there is no evidence that SNRs are preferentially located at the sites of densest molecular gas measurable by this ratio at 50 pc resolution.

A notable exception is the compact continuum source 44.01 + 59.6, one of the brightest in M82, and one which coincides with the position of the peak HCO^+/CO ratio in Figure 4. The source 44.01 + 59.6 and the associated peak in HCO^+/CO are located approximately 3″ southeast of the 2.2 μm peak identified by Dietz et al. (1986), and are therefore spatially distinct from the presumed IR nucleus. Note that the HCN map of Brouillet & Schilke (1993) also shows a local peak in brightness within about 1″ of the position of the compact continuum source.

The source 44.01 + 59.6 has been the subject of a recent suggestion that it is associated with the active galactic nucleus (AGN) in M82 (Wills et al. 1997; Seaquist, Frayer, & Frail 1997). This view is prompted by its unusual radio spectrum (with a positive spectral index), a strong low-frequency turnover (Wills et al. 1997), and the possible detection of an associated jetlike structure (K. Wills 1997, private communication). The identification of 44.01 + 59.6 as the AGN source is supported by observations by Seaquist et al. (1997) that the satellite OH lines at 1612 and 1720 MHz associated with this source exhibit strong conjugate emission/absorption similar to that found in the AGN source of Cen A (van Langevelde et al. 1995) and in the nuclear region of NGC 253 (Frayer, Seaquist, & Frail 1998). No other source in M82 exhibits this characteristic, even though some other compact sources are brighter than 44.01 + 59.6. The inference is that the continuum source lies behind (or within) a region of gas with a locally very high column density of dense molecular gas, which is in agreement with our HCO^+ measurement. Note that a similar association between an AGN and high-density molecular gas, but using HCN as a tracer, is found in the prototype Seyfert galaxy NGC 1068 (Helfer & Blitz 1995). It should be noted that in M82, however, the high ratio of HCO^+/CO

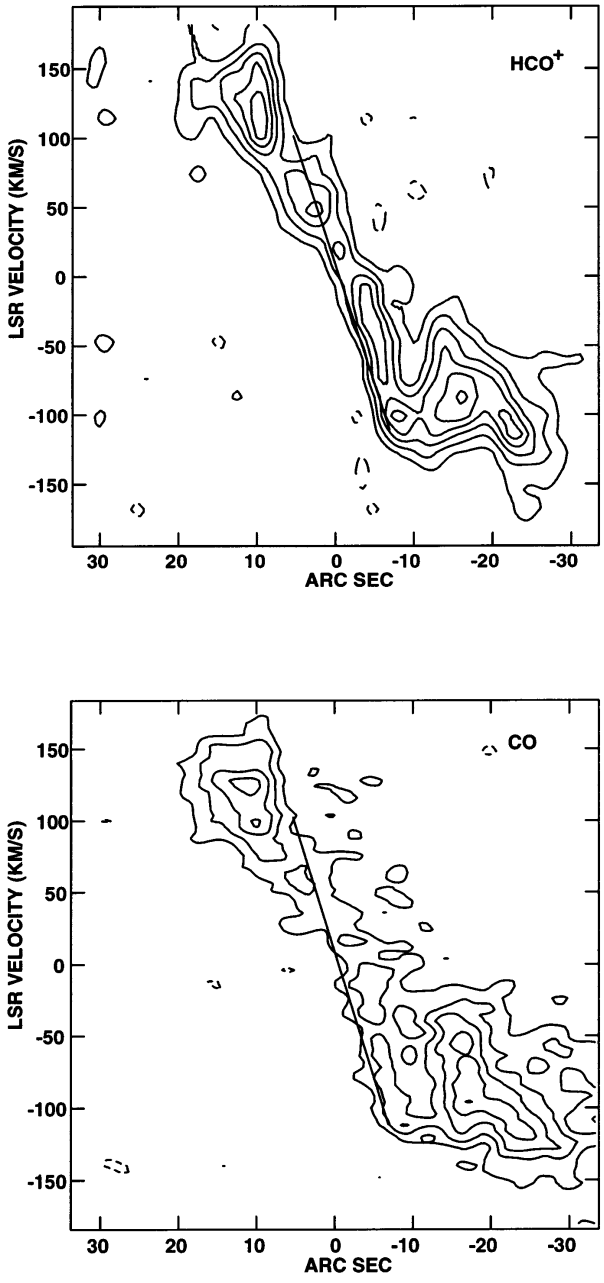

FIG. 2.—Position-velocity plots of HCO^+ (1–0) (*top*) and CO (1–0) (*bottom*) emission in M82. The latter plot is adapted from Shen & Lo (1995), convolved to the angular resolution of the HCO^+ data (3″.50 × 3″.25). In each case the horizontal axis corresponds to angular displacement (east is positive) along the major axis at P.A. = 75° passing through the IR nucleus defined by Dietz et al. (1986). The reference coordinates correspond to the location of the IR nucleus and $V(\mathrm{LSR}) = 200$ km s^{-1}. The contours are at uniform spacing with interval 0.406 K for HCO^+ and 4.86 K for CO. The diagonal line marks the location of the model for the ionized ring by Achtermann & Lacy (1995).

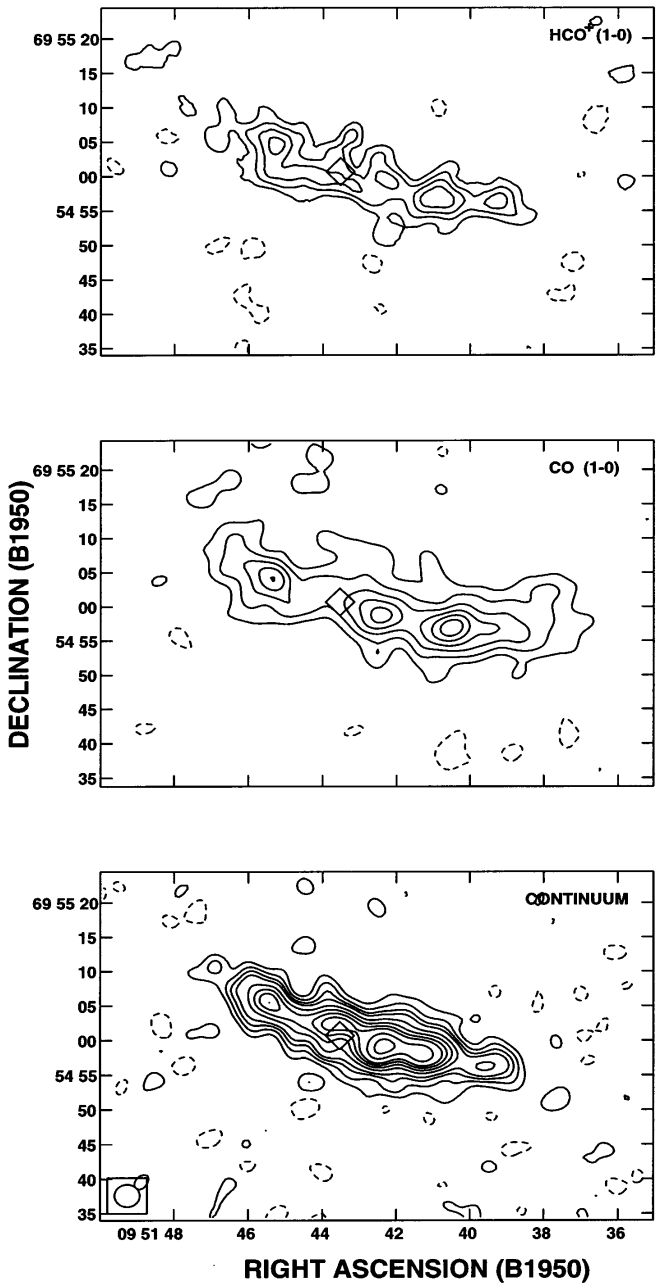

FIG. 3.—Three maps, each at angular resolution 3″.50 × 3″.25, showing the brightness integrated over velocity for HCO^+ (1–0) with uniform contours at intervals of 40.6 K km s^{-1} (*top*), the integrated brightness for CO (1–0) with uniform contours at intervals of 324 K km s^{-1} adapted from Shen & Lo (1995) (*middle*), and 3 mm continuum, with contours as in Fig. 1 (*bottom*).

could be attributable either to a high gas density in the nuclear region or to ionization effects associated with the suspected AGN source. It should also be noted that, if this source is the AGN, it appears displaced both with respect to the IR nucleus and with respect to the apparent major axis of the maps in Figures 3 and 4.

3.1.4. *Comparison with* OH

We have also searched for coincidences between high HCO^+/CO ratio and regions of enhanced 1720 MHz satellite maser emission in the nuclear region of M82 observed by Seaquist et al. (1997). Features of this type are found to be associated with 10% of radio SNRs in our own Galaxy (Frail et al. 1996), and with the source Sgr A East in the nuclear region of our Galaxy (Yusef-Zadeh et al. 1996). The 1720 MHz emission is believed to be preferentially excited in regions of dense collisionally excited gas in SNR shocks. Three 1720 MHz sources were found by Seaquist et al. (1997), omitting one south of the plane of M82, which may be spurious. None of these three coincide with observable enhancements in the HCO^+/CO ratio. However, we call attention to feature 2 in Seaquist et al. (1997), which is the

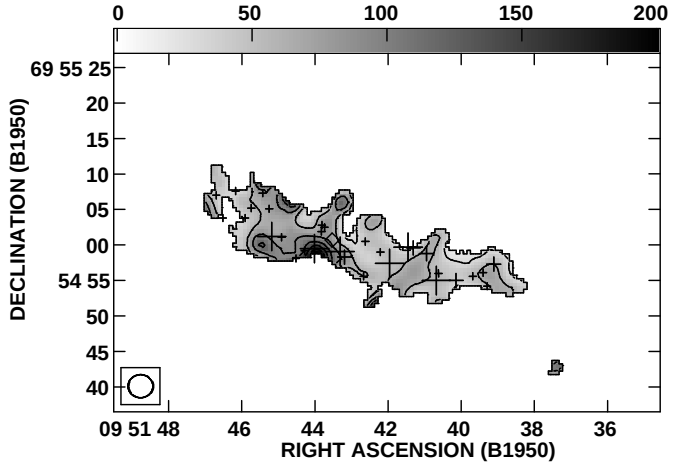

FIG. 4.—Map of the ratio HCO^+/CO, using the maps in Fig. 3, showing also the distribution of radio SNRs (*crosses*) and the IR nucleus, as in Fig. 1. Regions where the CO emission is fainter than 3 are blanked. The contours are uniform with an interval of 0.05. The gray-scale axis shows the milliratio.

most intense 1720 MHz feature, and is located roughly midway between two discrete continuum sources. One of these, the brightest and most compact source 41.95 + 57.5, is about 1″ northweat of the maser. It is also nearly identical in position and velocity with the main line 1667 MHz maser m2 identified by Weliachew et al. (1984). Figure 6 shows a comparison among the OH and the HCO^+ (1–0) profiles (measured at the position of the 1720 MHz feature). The profiles of all three features are similar, suggesting an association between the dense gas exciting the 1720 MHz line and the HCO^+ line. The density of H_2 responsible for the OH emission may therefore be comparable to the critical density for the HCO^+ line, or about 10^5 cm^{-3}.

3.1.5. *Comparison with 3 Millimeter Continuum*

We have also made a quantitative comparison between the 3 mm continuum and the HCO^+ (1–0) and CO (1–0) integrated line intensities. The millimeter continuum is predominantly free-free emission and is thus sensitive to the emission measure associated with ionized gas, and thus with star-forming regions. Since the 3 mm emission is optically thin, its brightness is a measure of the star formation rate integrated along the line of sight. The concentration of molecular gas is also expected to be higher in star-forming regions, and thus the brightness in HCO^+ and CO should reflect the distribution of these regions. Thus a correlation between continuum and molecular gas would be expected. However, a general correlation is also anticipated simply because a higher brightness of all such features is associated with the nuclear disk (e.g., the brightness for all features goes to zero at the edge of the disk). Therefore we focus on the search for a *nonlinear relationship* between continuum and molecular line emission, which might be expected in association with the Schmidt law (see discussion in § 4.2).

Figure 7 shows four plots, two for each molecule: one at the angular resolution of our HCO^+ (1–0) data, and the other smoothed to angular resolution 10″. The two plots for CO show a relationship whose scatter decreases with lower resolution, the effect of smoothing over a stochastic component, or "noise." The "noise" is not instrumental but

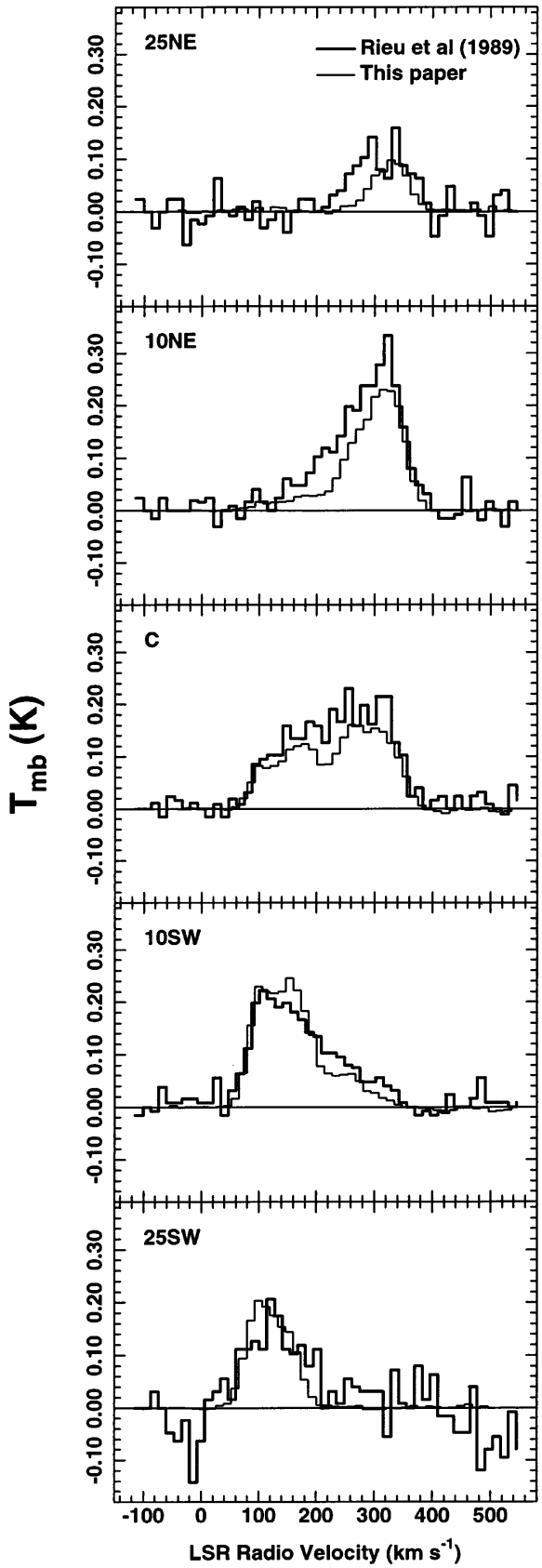

FIG. 5.—Comparison of line profiles of HCO^+ (1–0) measured by Rieu et al. (1989) using a single-aperture radio telescope (*thick lines*) and corresponding profiles from our own interferometer measurements (*thin lines*) at five different positions in M82. The interferometer data cube was convolved to the same angular resolution (23″) as the single-dish measurements for the purpose of generating the profiles based on OVRO data.

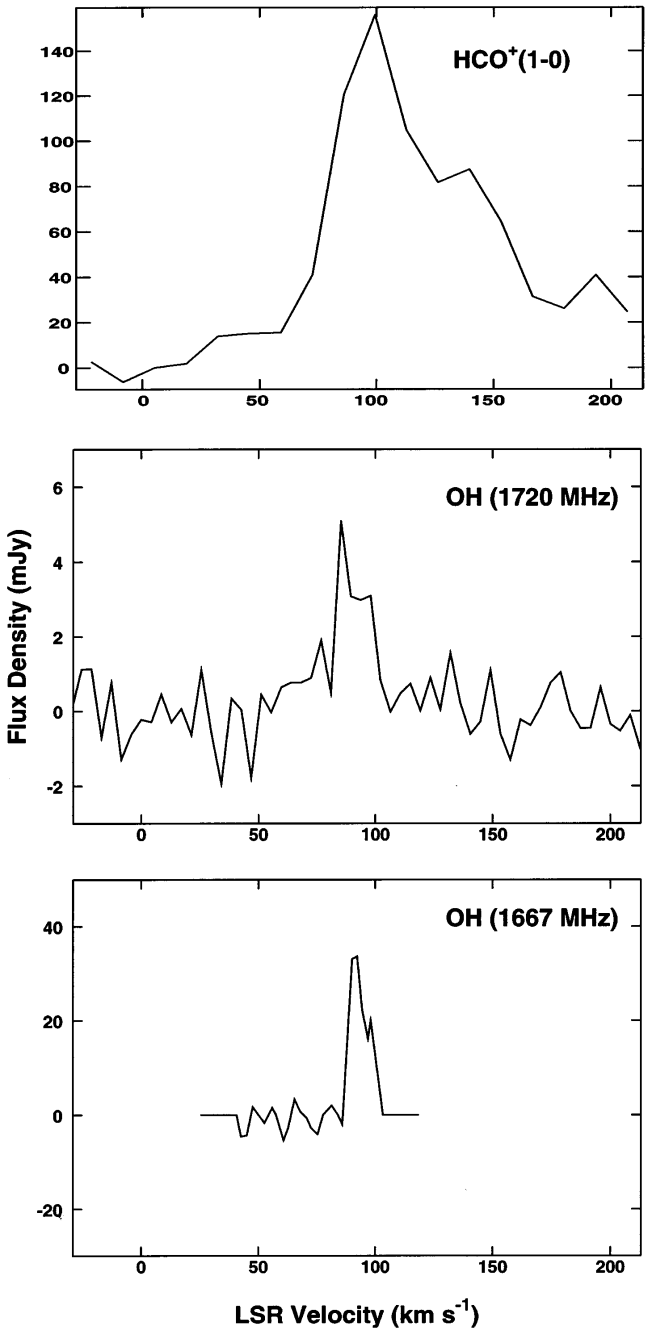

FIG. 6.—Comparison of spectral profiles for HCO^+ (1–0) from this paper (*top*), OH (1720 MHz) from Seaquist et al. 1997 (*middle*), and OH (1667 MHz) from Weliachew et al. (1984) for the OH maser region near the radio SNR 41.95 + 57.5 (*bottom*). The HCO^+ measurements have an angular resolution of 3″.5, whereas the OH measurements have an angular resolution of approximately 1″.

represents a real decorrelation in the data on scales less than about 100 pc. This is particularly noticeable in the CO map, where the amplitude of the noise scales clearly with the average brightness level. The level of the instrumental noise is indicated by the negative amplitudes at the origin. The case for HCO^+ is less clear, because the signal-to-noise ratio is lower.

The plots based on smoothed data appear to exhibit a nonlinear relationship between line and continuum brightness. We have therefore used these plots to search for the parameters of a fit of the form $\log \Sigma_R = \text{constant} + N \log \Sigma_G$, where Σ_R and Σ_G are respectively the continuum and line brightness (with negative values excluded). A variety of methods outlined by Akritas & Bershady (1996) were used to fit the data. These methods allow a solution for the parameter N and its uncertainty when both independent and dependent variables are subject to error. The results for HCO^+ and CO are $N = 1.17 \pm 0.16$ and $N = 1.29 \pm 0.10$, respectively. Both plots exhibit $N > 1$, signifying a higher than linear dependence, but only the result for CO appears significant. We note that a similar power-law relationship exists for Hα surface brightness versus total gas surface density for other galaxies, where it is found that $N \sim 1.3$–1.4 (e.g., Kennicutt 1990, 1998). We return to this point in § 4.2.

3.2. *The* HCO^+ (4–3) *Data*

The HCO^+ (4–3) data obtained with the JCMT are shown in two forms. Figure 8 shows a grid of all the line profiles together with the OVRO profiles for HCO^+ (1–0) at the corresponding positions. The latter profiles were generated from the spectral line cube of the OVRO data after first convolving the latter to the angular resolution of the HCO^+ (4–3) data (14″) and converting the intensities to main-beam brightness temperatures. Figure 9 shows the *p-v* plots for both data sets along the major axis. Comparisons between these two transitions must be made with caution, since the OVRO measurements undersample the short spacings. The analysis in § 3.1.1 indicates that the OVRO intensities may be low by an average of 25%, more so on the east side. Nevertheless, the comparison provides information on the upper limits to the (4–3)/(1–0) ratio, and can provide a qualitative picture of any variations in the line ratio on small spatial scales.

Figures 8 and 9 indicate that there is a broad similarity between the distributions of HCO^+ (1–0) and HCO^+ (4–3) emission, implying that the mean excitation conditions are relatively uniform throughout the nucleus of M82. We examine this further by looking at the spatial variation of the line ratios, always bearing in mind the cautionary note in the previous paragraph. Integrated line ratios were computed for each position in Figure 8 by determining the numerical value of the scaling factor for the (1–0) profile which produces the best match to the (4–3) line in the least-squares sense. These values are noted in Figure 8, together with their errors. We have also computed the mean ratio weighted by the inverse square of the errors, which yields 0.39 with a dispersion (standard deviation) of 0.17. The dispersion is about twice the mean standard error (0.09) of the individual measured ratios. Much of the observed dispersion is attributable to a systematic increase in the ratio with position along the major axis, increasing from west to east. However, this trend may be attributable to undersampling of the *u-v* plane, suspected from the results of Figure 5, since there is evidence there that the line flux is underestimated on the eastern side of M82. Therefore this trend is probably not real. Note that there is some evidence for a similar trend in the HCO^+ (1–0)/CO (1–0) ratio, possibly resulting from a similar undersampling problem in the CO (1–0) map.

Finally, a careful examination of the *p-v* plots in Figure 9 reveals a small inward displacement (by a few arcseconds) of the peaks representing outer spiral arm emission (features E2 and W3) in HCO^+ (4–3) relative to that in HCO^+ (1–0). This may be related to a similar effect noted in § 3.1.2 in

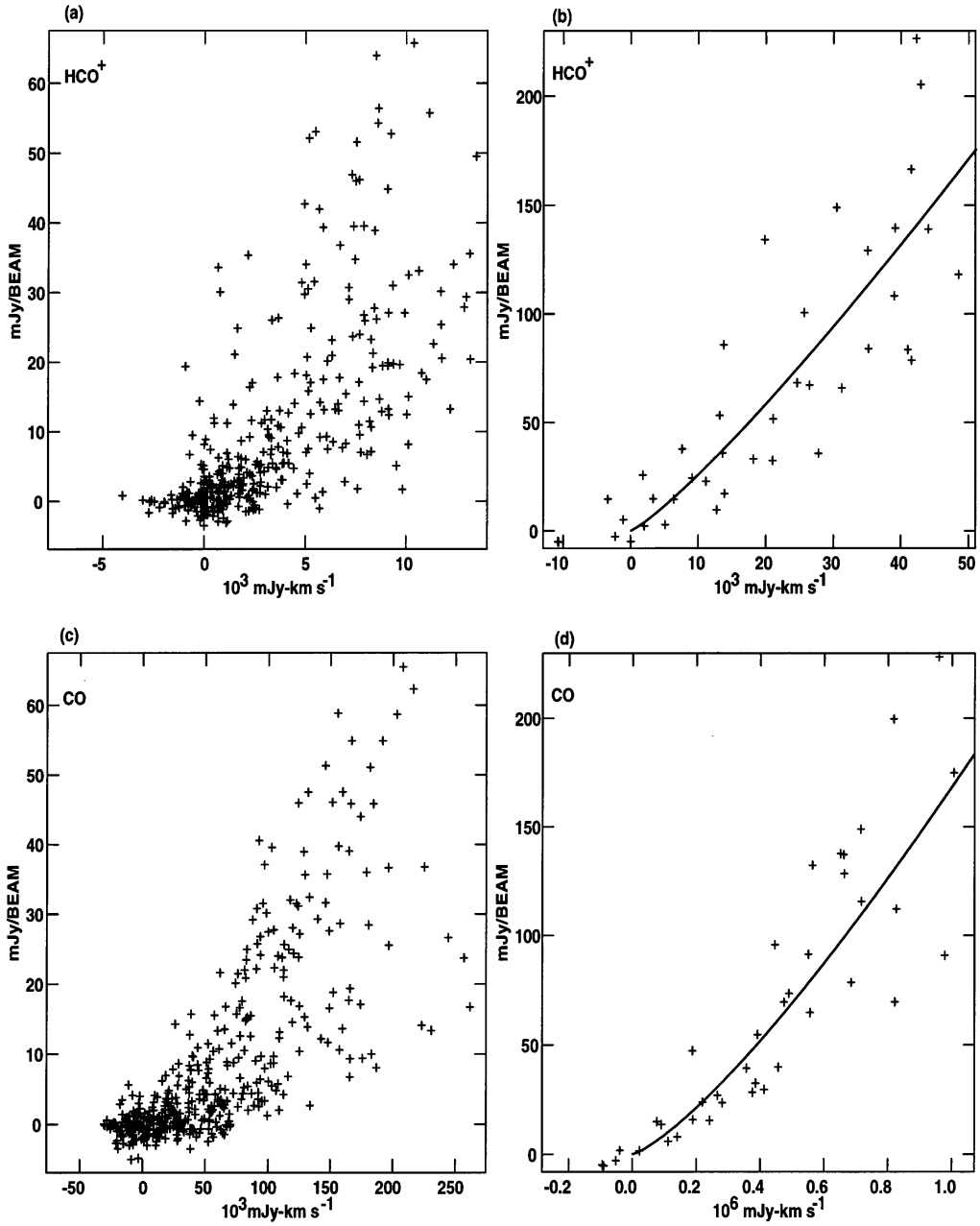

FIG. 7.—Plots of 3 mm continuum brightness (*vertical scale*) vs. integrated HCO^+ (1–0) and CO (1–0) emission (*horizontal scale*). Plots (*a*) and (*c*) were made using maps with the original angular resolution of the HCO^+ (1–0) measurements, and (*b*) and (*d*) were made using maps convolved to an angular resolution of 10″. Curves shown for the latter two plots are of the form $\Sigma_R = A(\Sigma_G)^N$, where $N = 1.17$ for (*b*) and $N = 1.29$ for (*d*).

connection with HCO^+ and CO. This point is discussed further in § 4.1.

4. DISCUSSION

4.1. *Kinematics of the Molecular and Ionized Gas*

Figure 2 shows the *p-v* plots along the major axis for HCO^+ (1–0) and CO (1–0), indicating the rotation curves for the molecular gas. Also superimposed is a line marking the corresponding diagram for the ionized ring identified from [Ne II] observations by Achtermann & Lacy (1995). There is clearly a strong qualitative similarity between the distributions of CO and HCO^+. This ridge, which is exceptionally linear and which possesses a large velocity gradient, is responsible for features C1 and C2 in the central region of the CO-integrated brightness map of Shen & Lo (1995). The ionized gas feature is more closely aligned with this ridge than with the general distribution of molecular gas, but appears blueshifted with respect to this ridge, by up to 30 km s^{-1}. This displacement is confirmed by a similar displacement between H41α and HCO^+ (1–0) noted by Seaquist et al. (1996). The inference is that the steep ridge is associated with molecular and ionized gas and star formation. This interpretation is supported by the observed distribution of 1720 MHz OH line masers associated with radio SNRs in M82, which also follow this ridge and the zone where HCO^+ is most prominent. The appearance of a comparable structure on the east side is not evident. The indication is therefore that star formation is especially active on the west side of M82.

Based on their computations of orbits in the nuclear region, Achtermann & Lacy (1995) note the similarity

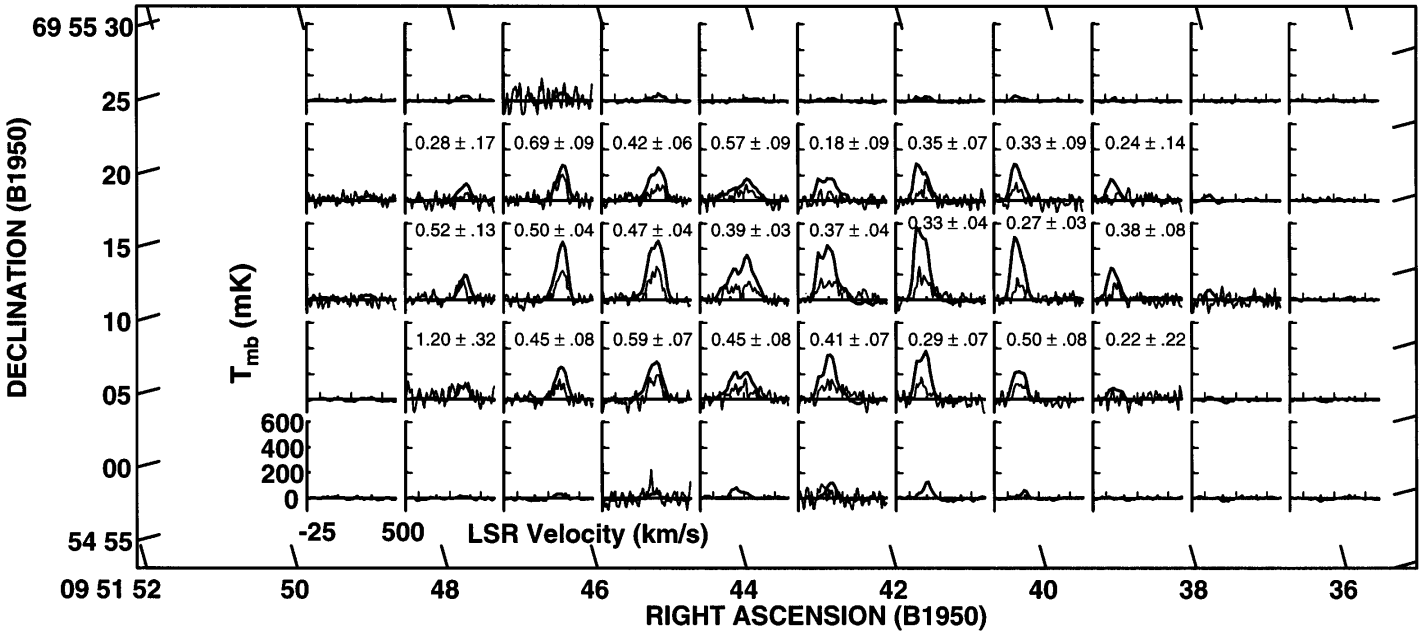

FIG. 8.—Map showing HCO^+ (1–0) and HCO^+ (4–3) profiles for M82, and the ratios (4–3)/(1–0) of the integrated intensities, with their errors (see text for details). The data cube for the (1–0) transition was convolved to the same angular resolution as that for the (4–3) transition (14″) before constructing the profiles. The coordinates for each panel refer to the origin of the plot.

between the *p-v* plot of the ionized ring and the $x2$ orbits of gas responding to the gravitational field of the bar, which appear significantly steeper than the larger $x1$ orbits defining the solid-body portion of the rotation curve. The closely associated steep and linear part of the rotation curve seen in molecular emission probably has a similar origin. According to this interpretation, the velocity displacements between ionized and molecular gas would require that the ionized gas be located in the outermost $x2$ orbits, perhaps associated with gas transferred from the inner $x1$ (intersecting) orbits, signifying intense star formation caused by gas in the colliding orbits. Alternatively, Götz et al. (1990) attribute the kinematics seen in [N II] in part to outflow from the nuclear disk. In the latter picture, the observed negative displacement in velocity might be attributable to shocked ionized gas entrained in the outflow (see also Seaquist et al. 1996). Note, however, that their model assumes that the northern edge of the M82 disk is the near side, whereas Wills et. al. (1997) show new and convincing evidence that the southern edge is the near side, based on a study of the radio SNRs. Thus this model may require some revision.

As noted in §§ 3.1.2 and 3.2, the *p-v* plots in Figures 2 and 9 reveal a slight inward displacement (toward the nucleus) of the spiral arm peaks associated with denser and more highly excited gas relative to those associated with lower density (features E2 and W3 in the maps of Shen & Lo 1995). The magnitude of this displacement is about 3″ (45 pc). The effect is to produce a slightly steeper velocity gradient when measured by these features. This effect might indicate that, like the ionized gas, the denser molecular gas also follows orbits in transition between the inner $x1$ and the outer $x2$ orbits near the inner Lindblad resonance (see Fig. 16 of Achtermann & Lacy 1995). Such gas would have undergone collisions due to the intersecting $x1$ orbits leading to star formation. As noted earlier, there is also a significant displacement inward of HCO^+ in the integrated brightness and 3 mm continuum maps for the feature W3, which is probably related to the displacements seen in the *p-v* plots.

The HCO^+ observations thus provide evidence of gas falling inward toward the nucleus where star formation and hence ionization is more pronounced. Note that HCO^+ may also be excited by other effects (e.g., ion drift) or enhanced in abundance by ionization effects, each of which could also be enhanced in the region of transfer between the $x1$ and $x2$ orbits because of shocks created by cloud collisions.

4.2. *The Schmidt Law*

We noted in § 3.1.5 the existence of a nonlinear relation between the millimeter continuum and molecular line brightness, especially for CO. The former quantity is associated with the star formation rate and the latter with the molecular gas density, both integrated over the line of sight. Thus the relationship represents an alternative way of investigating the Schmidt law, i.e., the relationship between the local star formation rate and the associated gas density. In its original form the Schmidt law relates these quantities by a simple power law, $R = a(\rho_g)^n$ (Schmidt 1959), where a is a constant and $n = 2$. In external galaxies, the observables are projected surface densities, leading to the alternate form $\Sigma_R = A(\Sigma_G)^N$. The quantity Σ_R is measured by the Hα surface brightness, and Σ_G is obtained from CO and H I observations, which yield the gas column density.

The results based on observations of galaxies are reviewed by Kennicutt (1990). In the case of studies of spatially resolved observations of (near face-on) galaxies, $N \sim 1.3$ is found for gas densities exceeding the threshold value $\Sigma_G \sim 3\ M_\odot\ \mathrm{pc}^{-2}$, with the star formation being totally suppressed at column densities significantly below this value. New results by Kennicutt (1998) show that for

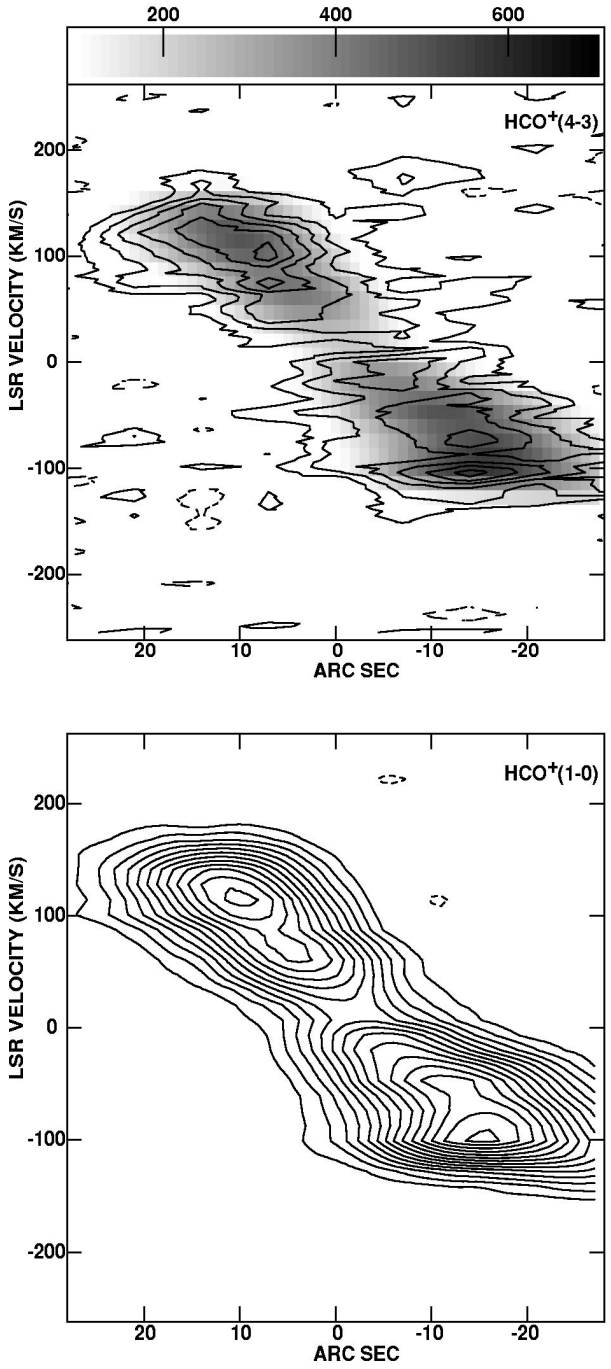

FIG. 9.—Position-velocity plots showing the distribution of HCO^+(4–3) emission (*top*) shown in contour form compared with a similar plot of HCO^+ (1–0) emission (*bottom*). The gray-scale image associated with the HCO^+ (4–3) plot represents the HCO^+ (1–0) emission in the lower panel for comparison. The HCO^+(1–0) emission was convolved to the angular resolution of the HCO^+ (4–3) data (14″). Contours for both plots are at uniform intervals of 0.04 K in T_{MB}.

globally averaged surface brightnesses applied to large samples of disk galaxies, $N \sim 1.4$. In M82 we find $N \sim 1.3$ using the measured CO brightness as a measure of total gas column density and the millimeter continuum surface brightness as a measure of the star formation rate (instead of Hα). Neither of the two variables measured is subject to significant interstellar extinction by dust through the disk. Note, however, that M82 is nearly edge-on instead of nearly face-on, so that it is not possible to directly infer the gas column density perpendicular to the disk. The column density measured perpendicular to the disk may, however, be estimated from the observed column density using a simple uniform disk model. The results indicate that the gas column density perpendicular to the disk significantly exceeds the threshold value shown above.

We have also investigated whether $N = 1.3$ is a reasonable value, assuming that the Schmidt law with $n = 2$ is valid, and that the observed surface densities are represented by integrals over the distributions of star formation rate and gas density. The effect of integrating along the line of sight is to sum the volume density of the star formation rate and gas over a statistical ensemble of variations in path length. The quantity N can be computed analytically if it is assumed that the path length is statistically correlated with the gas density (e.g., shorter path lengths are associated with higher density). If for example, we take $n = 2$, and represent the distribution of mean path length L as a Gaussian distribution of density {i.e., $L \propto \exp[-\text{const}\,(\rho^2)]$}, then we find $N = 1.5$, comparable to the value observed. Note that the value of N is not determined by whether the galaxy is nearly face-on or nearly edge-on, but instead by the form of the statistical relationship between mean path and density distribution in the regime above the critical surface mass density.

4.3. *Modeling the Line Ratios*

The line ratios shown in Figure 8 in principle yield information on the excitation conditions in the molecular gas. Our HCO^+ data alone are not sufficient to determine unique values of the excitation conditions, In addition, as noted in § 4.2, the line ratios are probably overestimated by about 25% because of incomplete sampling of the *u-v* plane. We therefore restrict our discussion instead to issues which do not depend critically upon the precise absolute numerical ratios, and to illustrative physical conditions. Figure 8 shows that the ratios vary comparatively little over the nuclear region and are all (within the errors) equivalent to the weighted mean value of about 0.4. Since the region observed would be expected to encompass a wide range of physical conditions, each sampling point must cover a similarly wide range of physical conditions, represented by an ensemble of a large number of molecular clouds, in which the average cloud is subthermally excited.

4.3.1. *Conditions in the Average* HCO^+ *Emitting Cloud*

To model illustrative physical conditions (averaged over the beam) satisfying the line ratios, we have assumed that the excitation is determined by the molecular abundance, gas density, and temperature only, and have used a standard large velocity gradient (LVG) approach to compare the expected line ratios with the ones observed. The collision cross sections used for HCO^+ are from T. S. Monteiro (1996, private communication), and include levels up to $J = 11$, with a correction for helium. We therefore ignore a variety of other effects that could influence the line ratios for HCO^+, discussed by Richardson et al. (1988). These other effects include collisions by electrons, ion drift (i.e., velocity differences between ionized and neutral species in the presence of a magnetic field), and radiative excitation by the millimeter continuum radiation field in M82. The LVG computations require knowledge of the parameter

$X(dv/dr)^{-1}$, where X is the abundance of HCO$^+$ relative to H_2, and dv/dr is the velocity gradient in the clouds. A number of analyses of HCO$^+$ have been performed in molecular clouds in our own Galaxy (e.g., Richardson et al. 1986, 1988; Heaton et al. 1993; Irvine, Goldsmith, & Hjalmarson 1987). Derived values for X fall in the range $1.0 \times 10^{-9} < X < 1.0 \times 10^{-8}$. Values of dv/dr (in km s^{-1} pc^{-1}) are generally near unity. For our calculations we employed $X(dv/dr)^{-1} = 1.0 \times 10^{-9}$. By computing line ratios for a series of densities and kinetic temperatures in the range 10^2–10^8 cm^{-3}, and $T_{\rm kin} = 20$, 40, and 60 K, we find that the ± 1 σ range in line ratios spanned by the observations (0.39 ± 0.17) is produced by densities in the range 1.8×10^4–1.6×10^5 cm^{-3}. This range of densities is comparable to those found by Seaquist et al. (1996) for the most dense ionized regions using the H41α line as a diagnostic.

In principle, the model brightness temperatures can be combined with the observed brightness temperatures to infer the geometric dilution factor F, which is determined by the product of the area covering factor and the velocity dilution factor. This would require the development of models involving more transitions to determine the densities and temperatures uniquely. However, we can again look at a set of illustrative conditions. For example, the peak (1–0) line brightness temperature in Figure 8 is about 0.6 K, just east of the IR nucleus, where the line ratio is about 0.33. If the kinetic temperature is 40 K, the LVG models yield a corresponding density of about 3×10^4 cm^{-3} and a model brightness temperature of 15 K, leading to a dilution factor of 0.04. Thus the slice through the image cube at this position must reflect a large number of clouds filling about 4% of the cube volume.

4.3.2. HCO$^+$ *and Models with Fractal Geometry*

The range of densities derived above (10^4–10^5 cm^{-3}) could be thought of as representing a set of mean conditions reflecting the HCO$^+$ emitting regions. The gas is likely to be very nonuniform in density, and a different approach using models with multiple components will ultimately be necessary for the interpretation of multiline data. The substantial uniformity of the line ratios implies that the beam does not resolve these components, and that each sampling point is measuring average conditions over an ensemble of compact clouds, whose statistical properties are quite uniform from point to point. Quiescent molecular clouds in our Galaxy appear to exhibit fractal structure incorporating a power law for the number density–mass relationship. As noted by Elmegreen & Falgarone (1996), an idealized (fractal) sample including all clouds and cloud clusters in the hierarchy should give a cloud mass spectrum with a power-law index $\alpha = -2.0$. Power-law relationships are also observed for the dependence of the average density and velocity dispersion of the clumps on their size (e.g., Zinnecker 1990). The range in cloud size covered by these relationships is about 10^{-2} to 10^2 pc, i.e., 4 orders of magnitude. These power-law relationships are believed to be governed either by turbulence or by self-gravitation. This structure may be causally related to the form of the initial mass function for stars (e.g., Elmegreen & Falgarone 1996; Elmegreen 1997).

Although a detailed discussion of such models is premature and beyond the scope of this paper, we report that in a preliminary investigation of such a model, we find that the HCO$^+$ line ratios are compatible with $\alpha = -2.0$, when the other power-law relationships are constrained to those characterizing quiescent interstellar clouds in our own Galaxy. Such models will be interesting to pursue when sufficient line data become available. We will discuss such models and their relevance in a forthcoming paper.

5. SUMMARY AND CONCLUSIONS

The analysis of HCO$^+$ observations for M82 shows that the HCO$^+$ (1–0) emission in M82 is distributed throughout the inner 1 kpc in a way broadly similar to that of CO, and reflects the distribution of star-forming gas. There are some differences with respect to CO that reflect its excitation by higher gas density, and possibly other effects such as ionization by cosmic rays or UV emission in star-forming regions. The HCO$^+$ (1–0) tends to concentrate more toward the inner edges of the spiral arms, similar to the ionized gas. This star-forming gas may represent material in the $x2$ orbits that are near the inner Lindblad resonance and are associated with the gravitational influence of the bar in M82. This gas may be the product of transfer from the $x1$ orbits, which have larger radii.

The distribution of HCO$^+$ (4–3) is similar to that of HCO$^+$ (1–0), except for a slight inward displacement of the material in the spiral arms, as revealed by the p-v plots. This inward displacement, together with a similar displacement of HCO$^+$ (1–0) relative to CO in the spiral arms, may be evidence for gas in transition between the $x1$ and $x2$ orbits, signifying an inward transfer of gas. The HCO$^+$ (4–3)/(1–0) intensity ratio is relatively constant over the extent of the inner kpc region, indicating mean H_2 densities in the range 10^4–10^5 cm^{-3} for kinetic temperatures in the range 20–60 K. This is similar to the maximum densities derived for ionized gas from recombination line studies.

The low filling factor and the relatively constant HCO$^+$ (4–3)/(1–0) line ratio suggest that each point in the map contains a large ensemble of clouds with relatively uniform statistical properties. A preliminary application of fractal-type models based on studies of quiescent molecular clouds in our own Galaxy shows that the observed line ratios are consistent with the mass spectrum of quiescent molecular clouds, provided that the physical gas density scales with the mean cloud density.

There is no apparent enhancement in HCO$^+$ relative to CO at the sites of the compact radio-emitting SNRs in M82, except for the source $44.01 + 59.6$, where the HCO$^+$/CO brightness ratio is exceptionally high. This supports other evidence from continuum and OH satellite line studies that this source is associated with an AGN in M82.

Finally, an investigation of the Schmidt law for star formation, using the 3 mm radio continuum as a measure of star formation rate, and primarily CO brightness as a measure of gas column density, shows that $N = 1.3$, commonly found for nearly face-on spirals, is also consistent with the behavior of the nuclear region of M82. The inclination of the galaxy is likely to be unimportant in determining this parameter, provided that the measured quantities are unaffected by absorption by dust in M82.

E. R. S acknowledges the support of a grant from the Natural Sciences and Engineering Research Council of Canada. We thank the staffs of the Owens Valley Radio Observatory and the James Clerk Maxwell Telescope for their assistance, and we thank Sandra Scott for help with the preparation of this manuscript.

REFERENCES

Achtermann, J. M., & Lacy, J. H. 1995, ApJ, 439, 163
Akritas, M. G., & Bershady, M. A. 1996, ApJ, 470, 706
Brouillet, N., & Schilke, P. 1993, A&A, 277, 381
Carlstrom, J. E. 1988, in Galactic and Extragalactic Star Formation, ed. R. E. Pudritz & M. Fich (Dordrecht: Reidel), 571
Dietz, R. D., Smith, J., Hackwell, R. D., Gehrz, R. D., & Grasdalen, G. L. 1986, AJ, 91, 758
Elmegreen, B. G. 1997, ApJ, 486, 944
Elmegreen, B. G., & Falgarone, E. 1996, ApJ, 471, 816
Frail, D. A., Goss, W. M., Reynoso, W. M., Giacani, E. B., Green, A. J., & Otrupeck, R. 1996, AJ, 111, 1651
Frayer, D. T., Seaquist, E. R., & Frail, D. A. 1998, AJ, 115, 559
Heaton, B. D., Little, L. T., Yamashita, T., Davies, S. R., Cunningham, C. T., & Monteiro, T. S. 1993, A&A, 278, 238
Helfer, T. T., & Blitz, L. 1995, ApJ, 450, 90
Götz, M., McKeith, C. D., Downes, D., & Greve, A. 1990, A&A, 240, 52
Irvine, W. M., Goldsmith, P. F., & Hjalmarson, Å. 1987, in Interstellar Processes, ed. D. J. Hollenbach & H. A. Thronson (Dordrecht: Reidel), 585
Kennicutt, R. C., Jr. 1990, in The Interstellar Medium in Galaxies, ed. H. A. Thronson, Jr., & J. M. Shull (Dordrecht: Kluwer), 405
———. 1998, ApJ, in press
Kronberg, P. P., Biermann, P., & Schwab, F. R. 1985, ApJ, 291, 693
Richardson, K. J., White, G. J., Monteiro, T. S., & Hayashi, S. S. 1988, A&A, 198, 237
Richardson, K. J., White, G. J., Phillips, J. P., & Avery, L. W. 1986, MNRAS, 219, 167
Rieu, N. Q., Nakai, N., & Jackson, J. M. 1989, A&A, 220, 57
Schmidt, M. 1959, ApJ, 129, 243
Seaquist, E. R., Carlstrom, J. E., Bryant, P. M., & Bell, M. B. 1996, ApJ, 465, 691
Seaquist, E. R., Frayer, D. T., & Frail, D. A. 1997, ApJ, 487, L131
Shen, J., & Lo, K. Y. 1995, ApJ, 445, L99
Stark, A. A., & Wolff, R. S. 1979, ApJ, 229, 118
van Langevelde, H. J., van Dishoeck, E. W., Sevenster, M., & Israel, F. P. 1995, ApJ, 448, L119
Weliachew, L., Fomalont, E. B., & Griesen, E. W. 1984, A&A, 137, 335
Wild, W., Harris, A. I., Eckart, A., Genzel, R., Graf, U. U., Jackson, J. M., Russell, A. P. G., & Stutski, J. 1992, A&A, 265, 447
Wills, K. A., Pedlar, A., Muxlow, T. W. B., & Wilkinson, P. N. 1997, MNRAS, 291, 517
Yusef-Zadeh, E., Roberts, D. A., Goss, W. M., Frail, D. A., & Green, A. J. 1996, ApJ, 466, L25
Zinnecker, H. 1990, in Physical Processes in Fragmentation and Star Formation, ed. R. Capuzzo-Dolcetta et al. (Dordrecht: Kluwer), 201